



MAGNETIC MEASUREMENT OF FULL SCALE ENERGY DOUBLER
BENDING MAGNETS IN THE INITIAL STAGE
(E22-1 AND E22-13)

R. Yamada, H. Ishimoto and M.E. Price

April 6, 1977

1. Introduction

Since last summer, production of full scale bending magnets for the Energy Doubler is going on at a rate of 2~3 completed and canned magnets per month. The first 6 magnets (E22-1~6) have round beam bores and the next 7 ones (E22-7~13) have elliptical bores. Both of these have the returning 2 \emptyset lines inside the magnet coil. But, in the latest version (E22-14 series), the beam bore will be diamond shape and the 2 \emptyset line will be put outside the 1 \emptyset can to optimize heat exchange between the 1 \emptyset and 2 \emptyset lines and to reduce the heat load on the 1 \emptyset line. Efforts continue to suppress mechanical deformation of the magnet during high field excitation¹. So far, four types of stainless steel collars have been tried to improve the mechanical properties.

In this note, the detailed test results of two typical full scale E/D bending magnets in the initial stage (E22-1 and E22-13) are reported. To make comparison between the two easier, various parameters are summarized in Table I. The first full scale magnet (E22-1) was tested in the protomain tunnel last August using the existing test pump loop and the Gardner refrigerator². Since then, this cooling system had a lot of trouble and it was found uneconomical to operate such a big system for testing only one magnet. Early this year, decision was made to switch the cooling system to a recently completed prototype satellite refrigerator. The next E22-13 was cooled down with it at Lab.2³. Both magnets have not been trained up to their highest fields due to a short

between the coil and the ground for the E22-1 and due to too high a pressure rise in the cryostat at quench for the E22-13. However, most of the other key measurements were done for both magnets and the results of ac loss and field measurements are presented. At B-12, P. Limon et al excited the E22-7 up to 4500 A, corresponding to 44.1 kG.

2. Magnet Performance

Both magnets were cooled down with the refrigerator systems similar to that of the final Energy Doubler. Fig. 1 shows a schematic flow diagram which was used for testing the E22-1 magnet. In the recent test, the pump dewar and loop are eliminated. The satellite refrigerator was directly connected with the end box of the magnet system. The operating conditions for both cases were as follows:

	<u>E22-1</u>	<u>E22-13</u>
1 \emptyset inlet temperature	4.50 K	4.90 K
1 \emptyset outlet temperature	4.83 K	5.05 K
1 \emptyset pressure	11.3 psig	12.5 psig
2 \emptyset outlet temperature	4.66 K	4.5 K
2 \emptyset pressure	7.5 psig	5.2 psig

The high temperature operation for the E22-13 was found to arise from heat short between the shield line and the 1 \emptyset - 2 \emptyset lines. This problem may be solved in the next test run.

2-1 Quench Behavior

The E22-1 magnet had a short between coil and ground at voltages higher than 200 V. After all the necessary measurements, the magnet was quenched only 6 times due to limited time. Its quenching current was random. This may be due to a cavitation in the subcooled helium, which should not exist. The maximum field of this magnet was 36.3 kG.

The other E22-13 magnet had a quench inducing heater (25Ω) on the surface of the conductor outside the coil. The quench behavior was systematically investigated at the low current below the critical current (I_c) using the CAMAC-PDP-11 system described elsewhere². The current, the resistive voltage across the magnet, the voltage across the dump resistor of 0.2Ω , the energy dumped in the magnet, the resistance of the magnet and the upper limit of magnet temperature are shown as a function of time in Figs. 2~5. The integrated dumped energy into the magnet reached the maximum at about 0.6 second. The resistance value reaches a maximum at 0.2 second and starts to decay at 0.7 second, indicating the coil is cooling down again. The pressure changes in the 1 ϕ and 2 ϕ lines for induced and natural quenches were recorded on a strip chart. As shown in Fig. 6, the maximum 1 ϕ pressure is reached in about 0.6 second, then rapidly decreases.

The maximum pressure in the 1 ϕ line, energy loss in the magnet, maximum magnet resistance and the upper limit of magnet temperature are given in Fig. 7 as a function of induced quenching current. Here, the upper limit of temperature was calculated in the adiabatic condition using the observed current decay and the prepared temperature dependence of copper resistance and heat capacity. At current below 3,000 A, the quenches caused only minor perturbations except for a heated spot in the wire. Recovery was very rapid. Above 3,000 A, there were rapid changes with increasing current, while the temperature leveled off. This leveling off reflects an increase of the heat capacity of the conductor at that temperature, and a decrease of the time constant of the whole system with an increasing resistance.

The natural quench at 4,260 A caused the 1 ϕ pressure increase up to 92 psia. The cryostat itself has not been designed to stand a pressure over 60 psia. We did not quench the magnet any more and concentrated on measuring the field quality. The maximum field obtained was 41.7 kG.

The power supply was tripped at several currents and the resultant data as shown in Fig. 8, compared against those for quenches. The two sets of data were very similar to each other. The eddy current loss in the normal metal due to tripping at 40 kG is calculated to be less than 10 kJ. This fact suggests that the trip at high currents (above 3,500 A) induces a quench in the coil.

3. AC Loss

The ac loss is a major contribution to the heat load of a magnet. The main part is due to hysteresis of the conductor and is independent of the ramp rate. Total loss, including coupling losses, was measured as a function of ramp rate and maximum magnetic field.

The ramp rate dependence is shown in Fig. 9 for the E22-1 and E22-13 magnets. The ramp rate dependence of the E22-1 is much stronger than that of the E22-13 magnet. This big difference might come from the wire itself, but the true cause needs to be further investigated.

The maximum field dependence at constant ramp rate is also given in Figs. 10 and 11. The E22-1 was not measured at any field above 20 kG. Up to that field, the loss increases almost linearly with the maximum field. However, the dependence of the E22-13 deviates from linear above 20 kG. This deviation corresponds to droop in the shape of the magnetization curve as shown in Fig. 12. This phenomenon arises from the fact that there is some coil deformation due to magnetic force at high field. A careful glance at the high field portion of the magnetization curve informs us that there is a slight iron saturation above 40 kG. The projected loss from 4.5 kG to 45 kG is roughly 550 Joules/cycle for a ramp rate of 50 GeV/sec. This results in a heat load of about 10 W per magnet or just over 1.5 W/meter of magnet. This value includes the effect of wire movement and will be reduced to 400 Joules/cycle with a solidier coil.

4. Field Measurement

4-1 Hall Probe Measurement

Field measurement with a Hall Probe was made to have a rough idea of the axial field distribution at the magnet end at 1000 A for the E22-1, as shown in Fig. 13. The effective magnetic end of E22-1 is 3.625" outside the iron end.

The remanent field was also measured for the E22-1 after excitation up to 15 kG. As shown in Fig. 14, there can be seen two bumps at the end; one comes from the iron lamination and the other from the coil end.

4-2 Stretched Wire

In production measurements, the magnetic vertical plane and the integral field value $\int B dl$ are other factors to be measured. A loop of 4 mil wire with fixed spacing of 1.004 in. between two centers of the wire was stretched through the warm bore. For each magnetic field ramp an output signal was integrated and displayed on the scope. To find the magnetic vertical plane, the stretched coil is vertically placed and its angle is adjusted until we get minimum signal. The angle of the coil is read. Then, by rotating it 90 degrees, we can measure integral field value. This method was applied only for the E22-1. The magnetic vertical plane of E22-1 was found to be roughly 0.4° tilt from the mechanical vertical plane. The magnetic length was found to be $254.66" \pm 0.7"$ for E22-1. Accuracy was not very good because the voltage was not read within 0.1% errors. All these operations were made manually at that time. Fully automatic procedures to find the magnetic vertical plane and the integral field value are now being developed and will be used in the next run.

4-3 Harmonic Analysis

Various order harmonics (4 pole, 6 pole, 8 pole and 10 pole) were measured in the DC mode from low field up to above 40 kG, taking into account the

history of excitation. Measurements were made using the Morgan coils (1.5" dia. and 40" long for the E22-1 and 1.0" dia. and 12" long for the E22-13). The field distribution on the median plane ($Z=0$) is defined as follows:

$$B_z(x) = B_0 (1 + b_1 x + b_2 x^2 + b_3 x^3 + b_4 x^4 + \dots)$$

$$B_x(x) = B_0 (a_1 x + a_2 x^2 + a_3 x^3 + a_4 x^4 + \dots)$$

b_n is the normal component and a_n is the skew component.

4-3-1 Central Region

Various coefficients for both magnets are given in Figs. 15~21, and summarized in Table II for increasing field. In this measurement, it is very important that the harmonic coil be in the real center of the magnet coil, instead of the bore. Eccentricity affects the results, especially on the 4 pole component. The higher order components are not so seriously affected as the 4 pole one. This problem was confronted in the measurement of the E22-13, where the 4 pole component showed an hysteresis curve as the 6 pole one. Because it has an elliptical warm bore, the centering was very difficult. Some corrections were made for the horizontal shift in the obtained results of the E22-13.

The field quality of the first E22-1 is very bad, but this is not surprising since it was not mechanically well designed and its G-10 top key was crushed during construction. The field quality of the recent E22-13 was improved by a factor of about 3~10, but is still worse than that of the precision magnet E5-1. The most probable causes of 4 pole components are the vertical eccentricity of the coil in the iron lamination and the asymmetry of the coil itself.

The normal 6 pole component shows a hysteresis loop, which is due to the magnetization of superconductor. The constituent coming from construction errors does not depend on the excitation field. The 6 pole component does not seem to be so sensitive to the coil deformation which was pointed out in the previous section.

4-3-2 End Region

The only 6 pole component at end portion over one foot in length was measured for the E22-13. The results are given in Fig. 22 and Table II. It is worse than in the central region by a factor of 5. However, over the whole magnet, the integral 6 pole component is $\sim 3.75 \times 10^{-4}/\text{cm}^2$ for the 22-foot in length magnet at 40 kG. Due to a long straight section, the end effect is diluted. The end portion of the inner layer of this magnet is spread out to decrease the highest field in the coil. There still might be better end configuration in viewpoint of the field quality.

4-3-3 Remanent Field Quality

The remanent field was also investigated by exciting the magnet up to a desired field and then gently decreasing the current to zero. Fig. 23 shows the results for both magnets. Iron remanent field is roughly 2 Gauss and did not have a big 6 pole component. The big remanent 6 pole component comes from the persistent current in the superconductor itself.

4-4 Transfer Function Measurement with NMR

The NMR technique was employed to know the exact field value of the E22-13 magnet. However, the field quality of this magnet was not very good. Even with the proton sample below 22 kG, no signal could be observed without signal averaging. The signal averager, which consists of the microprocessor, was developed in the lab for this purpose. The details of this equipment will be described elsewhere⁵. The obtained transfer function (G/A) is shown in Fig. 24 as a function of the central dipole field. It exhibits a small hysteresis arising from the magnetization effect of superconductors. The transfer function without this effect is 9.807 G/A, while the calculated value by S. Snowdon is 9.75 G/A without iron saturation.

Acknowledgements

We would like to thank the personnel of Magnet Measurement Group who

contributed to various stages of this work. We also express our gratitude to C. Rode and his group for operating the cooling system.

References

- ¹ A.V. Tollestrup et al: Contribution to Accelerator Conference in Chicago, March (1977).
- ² R. Yamada, H. Ishimoto and M.E. Price: IEEE Trans. on Mag., Mag-13, 86 (1977).
- ³ R. Yamada, H. Ishimoto and M.E. Price: Contribution to Accelerator Conference in Chicago, March (1977).
- ⁴ G. Kalbfleish, P.J. Limon and C. Rode: Contribution to Accelerator Conference in Chicago, March (1977).
- ⁵ R. Yamada et al: Contribution to Accelerator Conference in Chicago, March (1977).

TABLE I

	<u>E22-1</u>	<u>E22-13</u>
Conductor	Airco - not keystoneed	MCA - keystoneed
Collar	Type I	Type I
1 ϕ and Beam Bore	Round	Elliptical
Iron Lamination		
i.d.	7.5"	7.5"
height	10"	10"
width	15"	15"
length	248"	248"
End Configuration	Not spread out	Spread out
Coil Length	21' 7 $\frac{1}{2}$ "	
Current Safety Lead	Yes	No

TABLE II

HARMONIC COEFFICIENTS AT INCREASING FIELD (D.C)

I. E22-1 A

Harmonics	5 kG		10 kG		20 kG		30 kG		
	b_n	a_n	b_n	a_n	b_n	a_n	b_n	a_n	
20	-1.9	25.0	-1.8	24.0	-1.5	22.0	-1.1	20.0	$\times 10^{-4}/\text{cm}$
30	-10.0	-0.43	-9.4	-0.39	-8.3	-0.29	-7.2	-0.21	$\times 10^{-4}/\text{cm}^2$
40	-0.8	-34.7	-0.73	-31.8	-1.41	-26.0	----	----	$\times 10^{-5}/\text{cm}^3$
50	14.4	-0.74	13.7	-0.48	12.9	-0.12	----	----	$\times 10^{-6}/\text{cm}^4$

II. E22-13

Central Region

20	-1.61	-4.79	-1.04	-5.08	-0.69	-5.16	-0.38	-5.10	$\times 10^{-4}/\text{cm}$
30	-4.02	-0.49	-2.98	-0.48	-2.84	-0.45	-2.73	-0.43	$\times 10^{-4}/\text{cm}^2$
40	0.24	-1.39	-0.28	-1.60	-0.68	-1.25	-1.13	-1.22	$\times 10^{-5}/\text{cm}^3$
50	-7.63	0.08	-4.56	0.37	-4.59	-1.51	-4.08	-1.15	$\times 10^{-6}/\text{cm}^4$

End Region

30	-15.3	-1.61	-14.9	-0.1	-14.9	-0.1	-14.9	-0.1	$\times 10^{-4}/\text{cm}^2$
----	-------	-------	-------	------	-------	------	-------	------	------------------------------

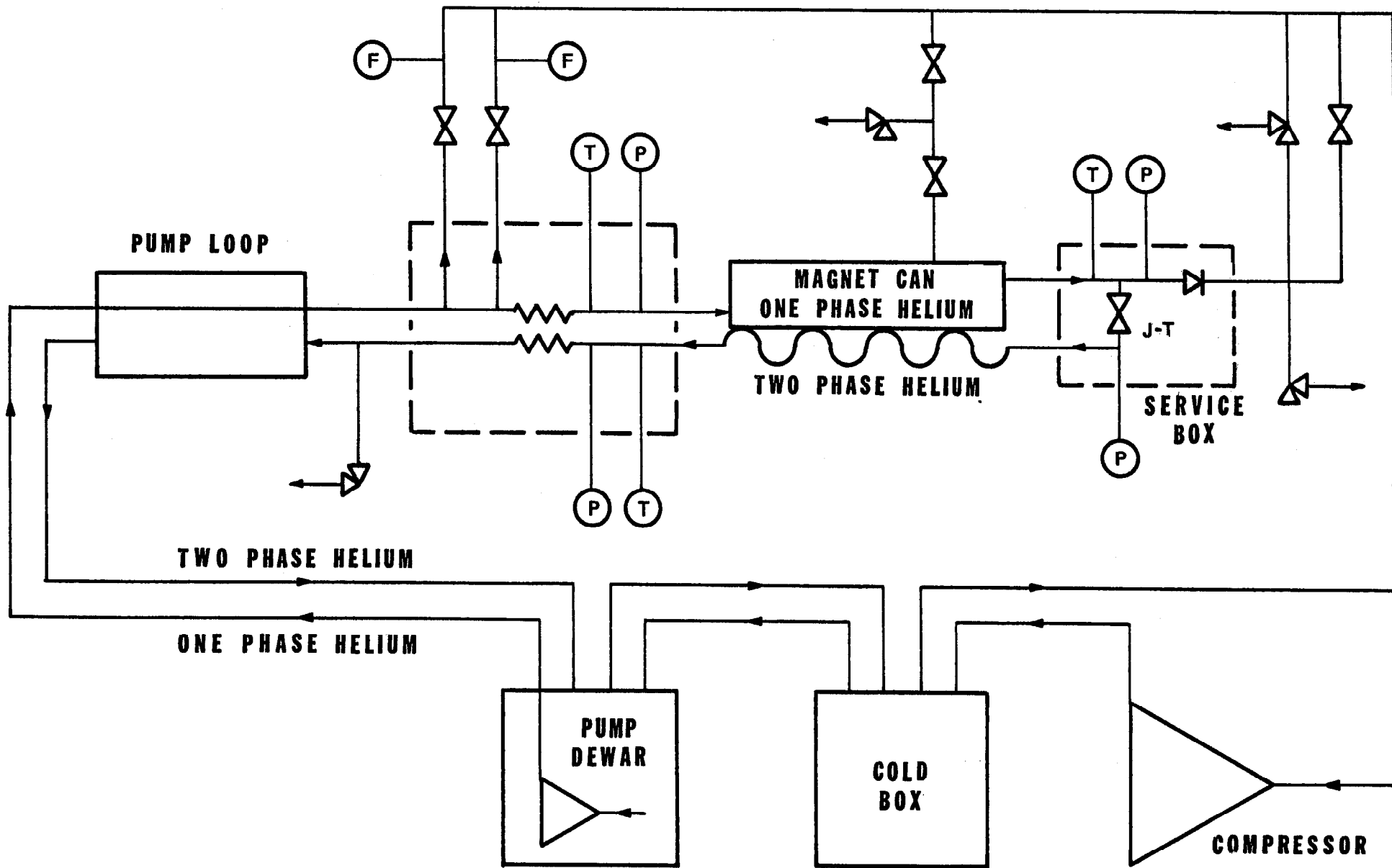


Fig. 1

REFRIGERATION SYSTEM OF MAGNET

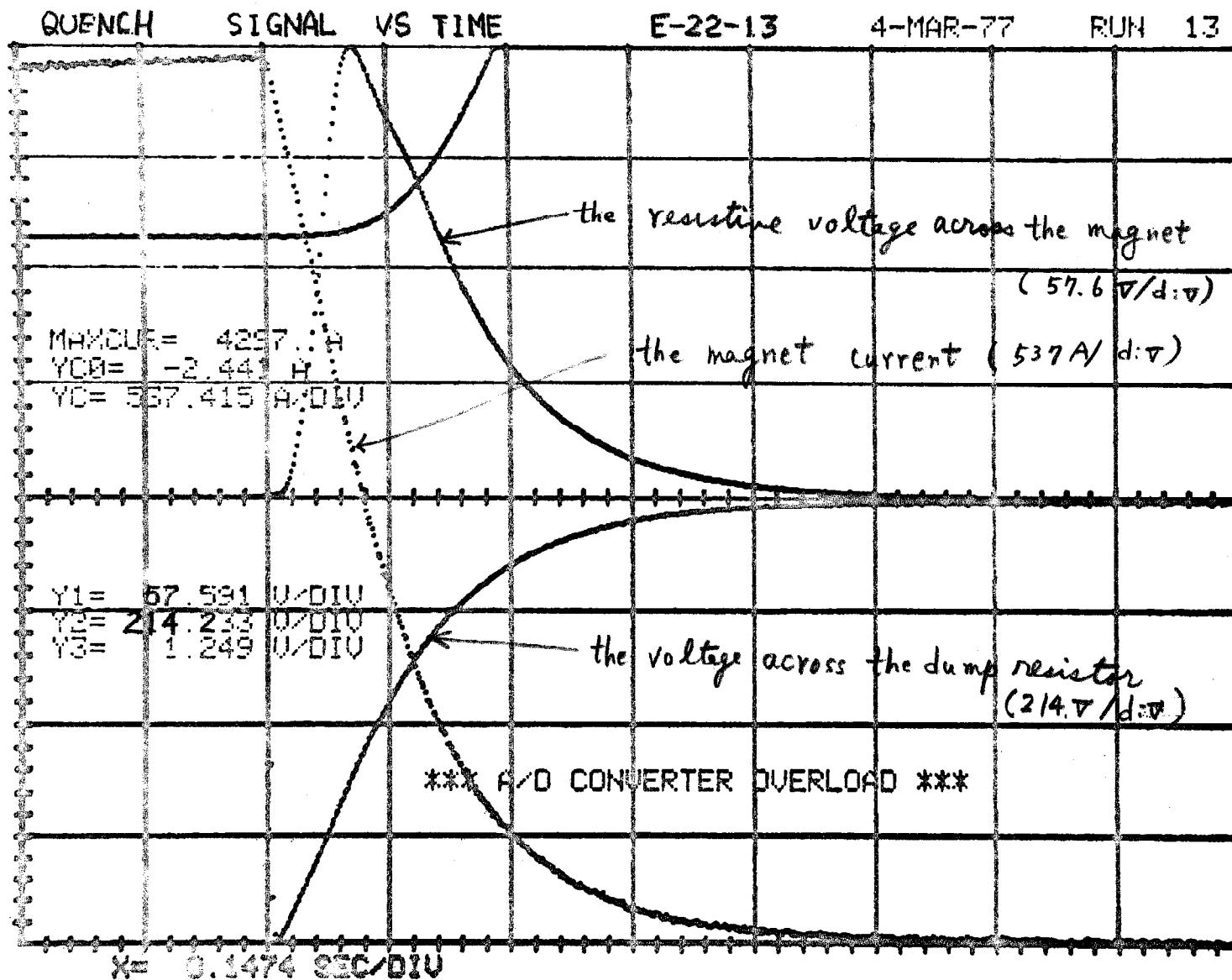


Fig 2 Various Parameters during quench as a function of time

Fig. 3

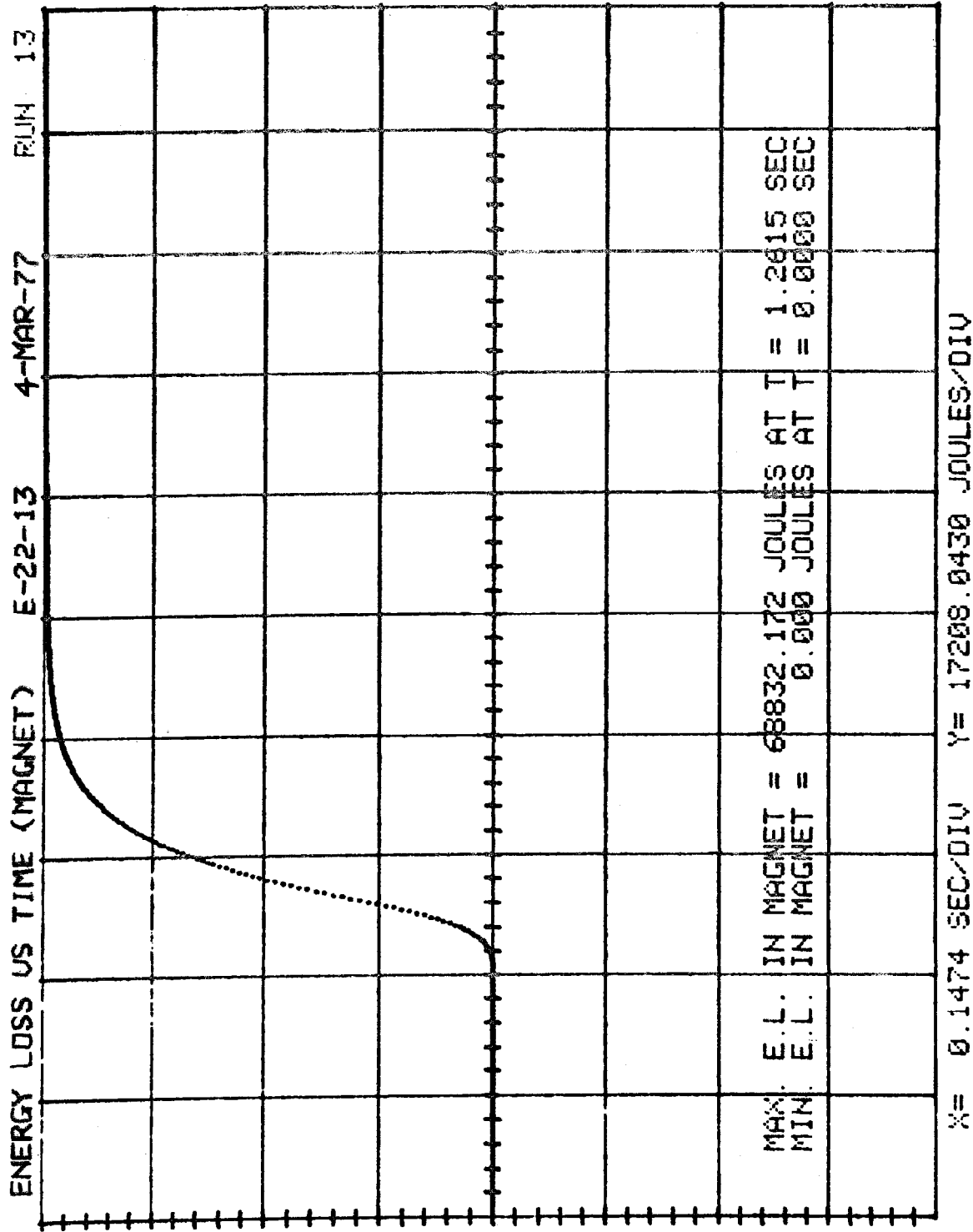
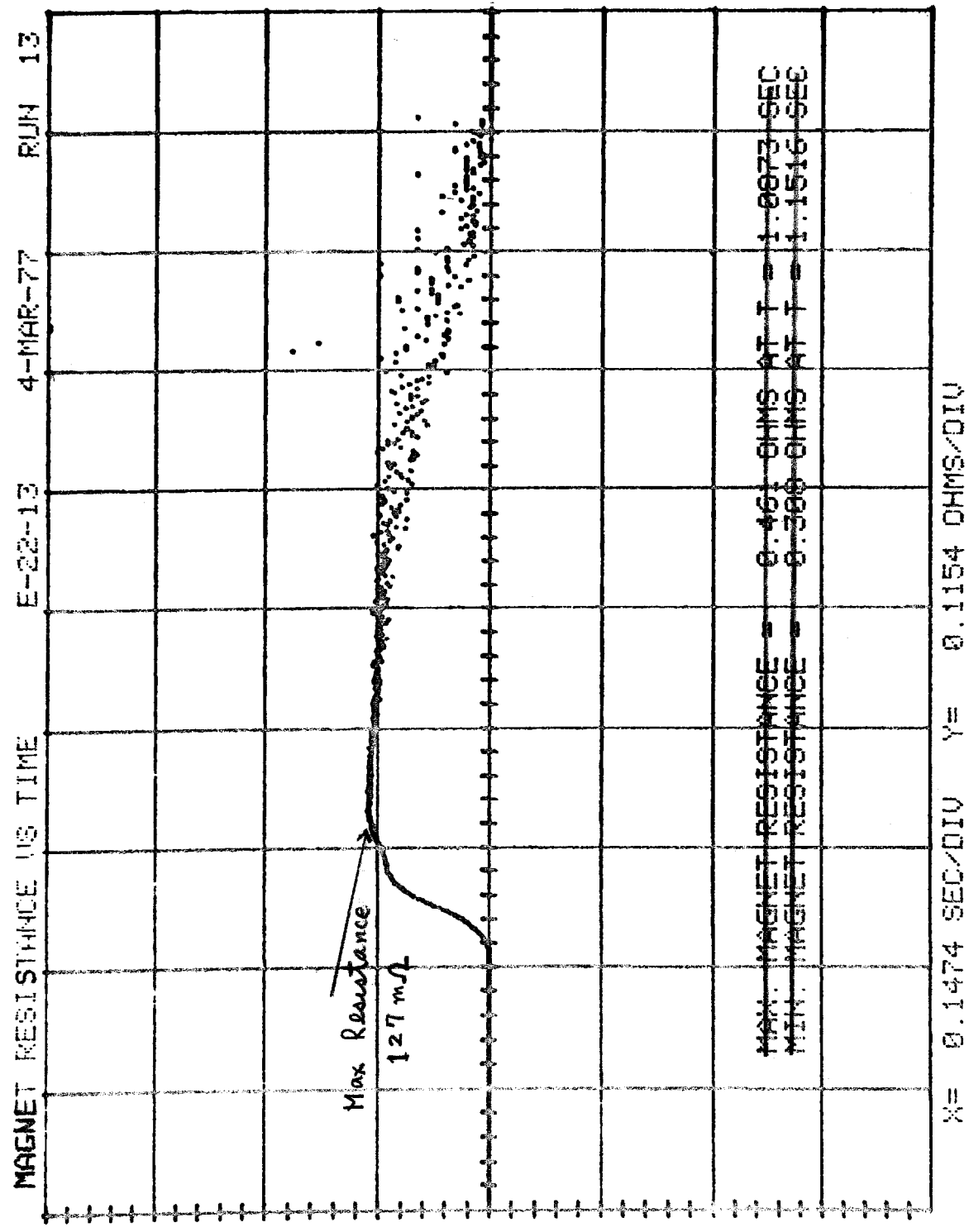


Fig. 4



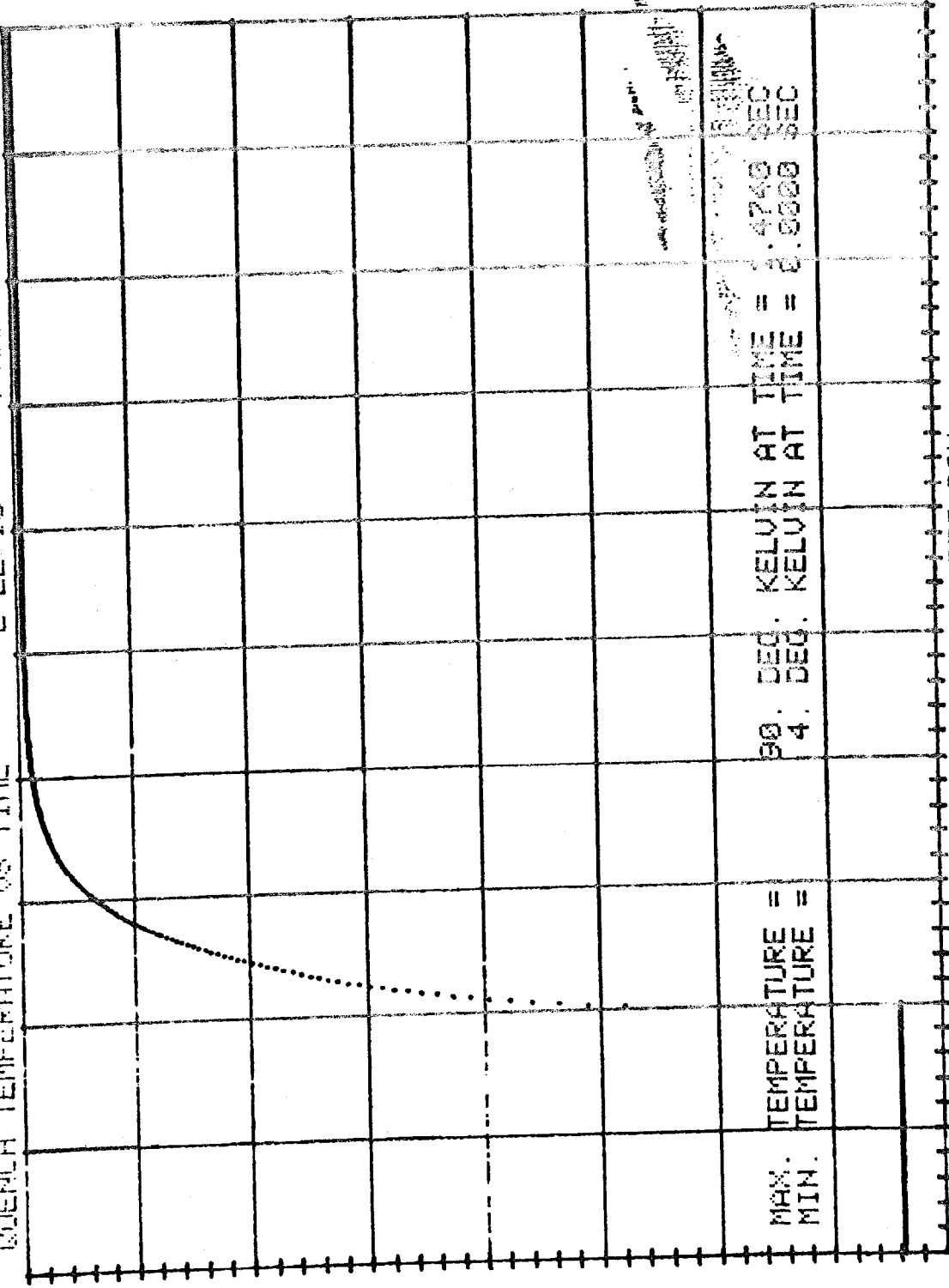
4-MAR-77

E-22-13

RUN 13

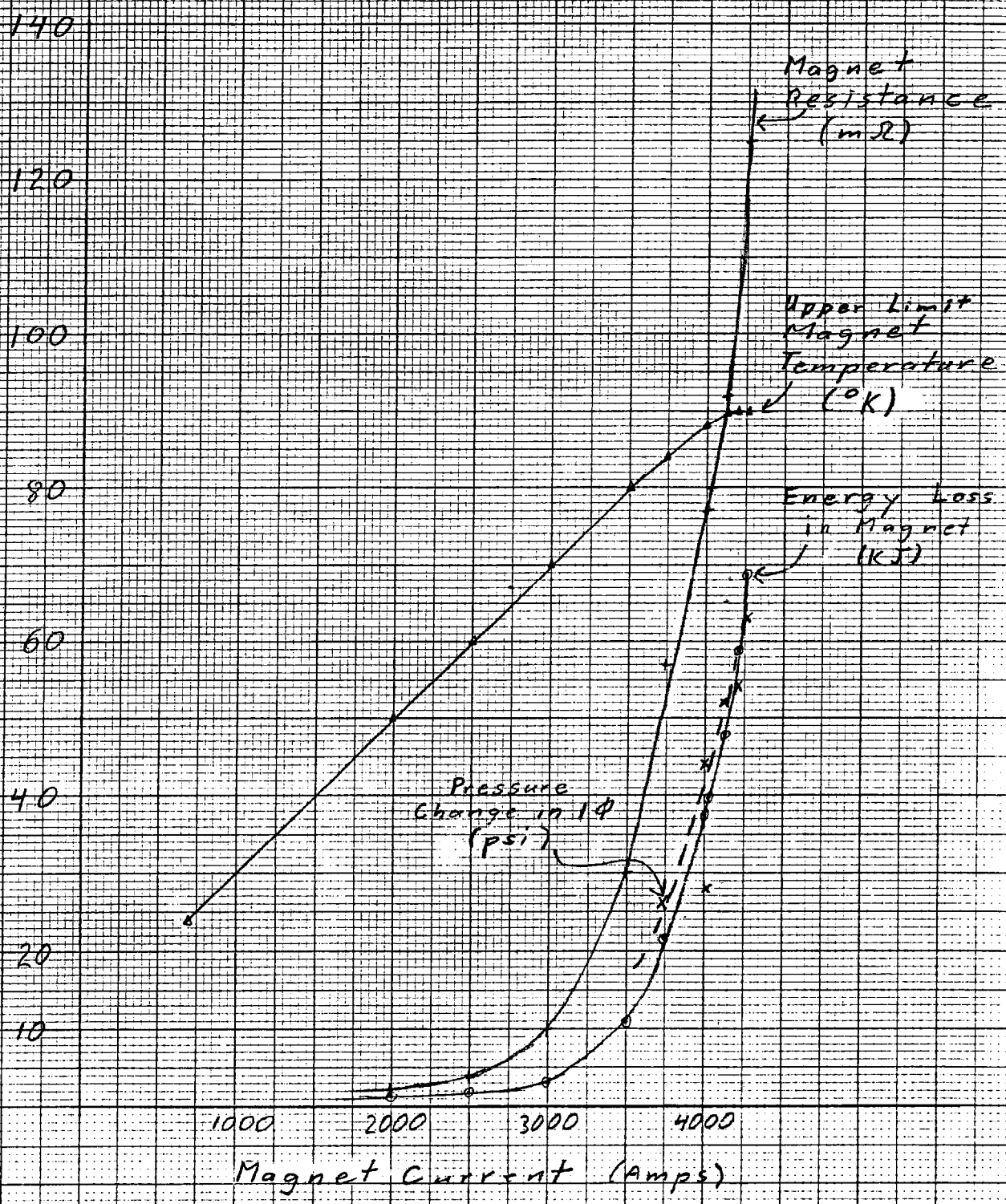
Fig. 5

QUENCH TEMPERATURE VS TIME



March 5 1977

Fig. 7 Magnet Parameters Heat Quench



March 5 1977

Fig 8 Magnet Parameters Trip

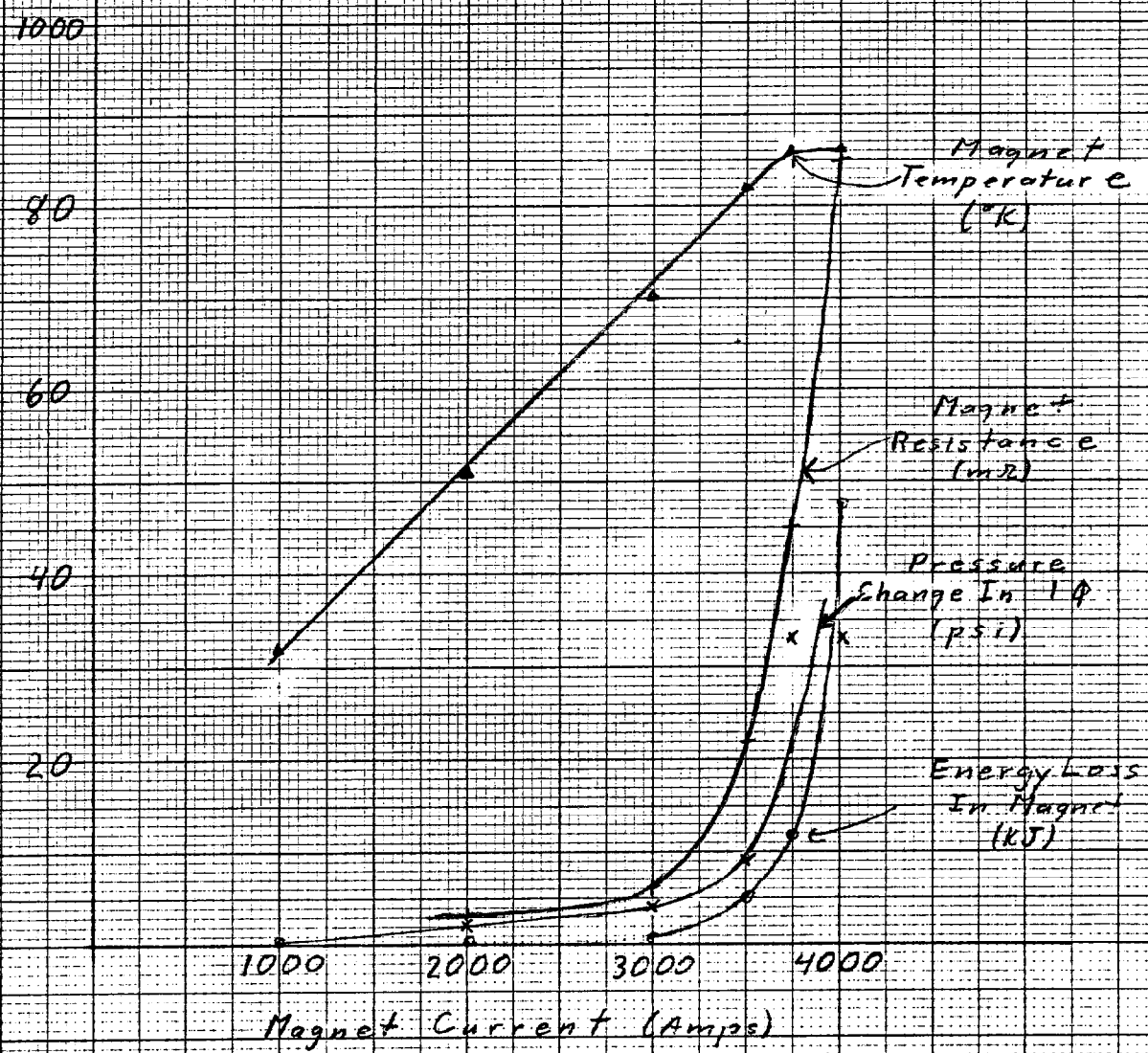
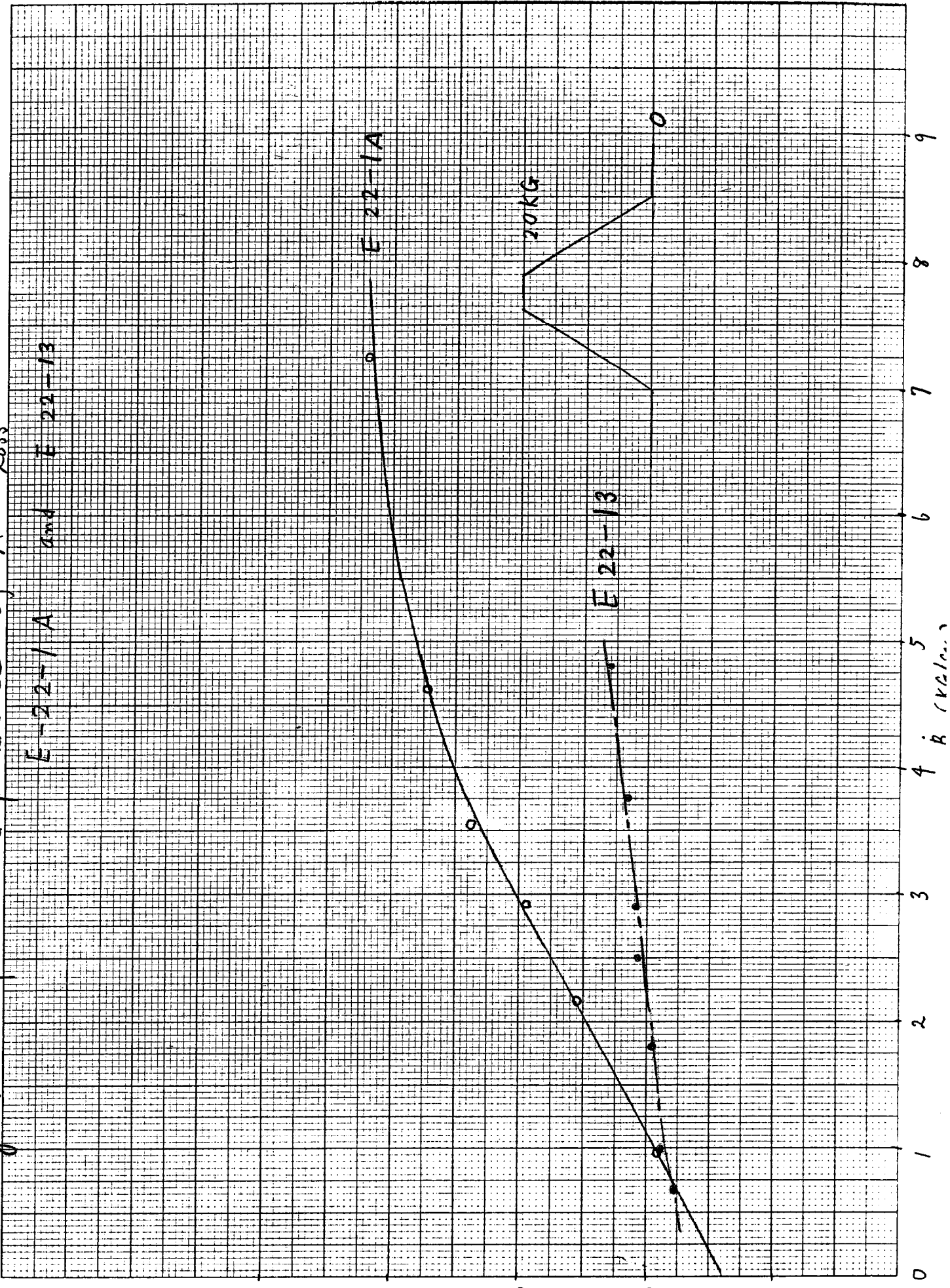
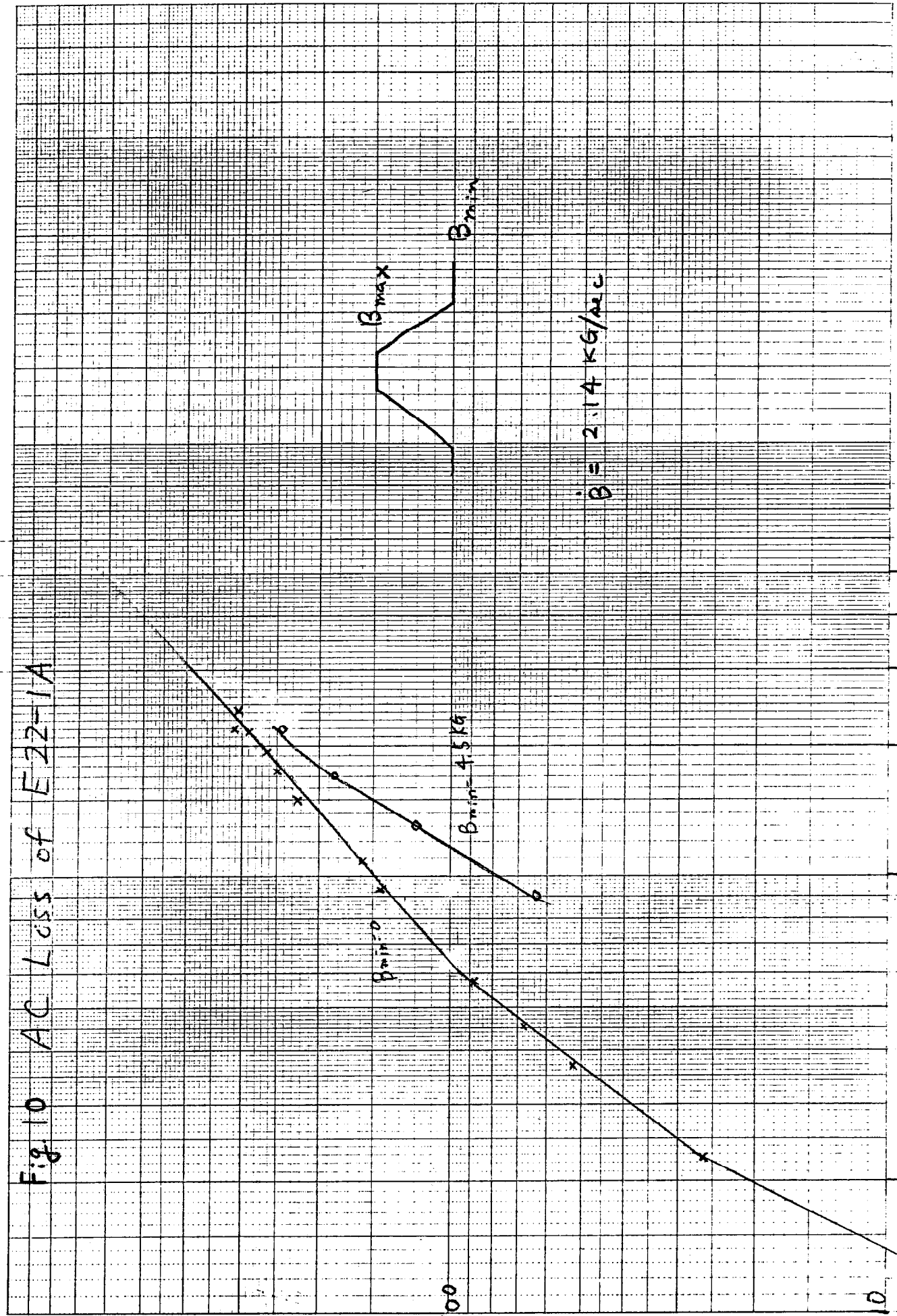


Fig. 9 Ramp rate dependence of AC Loss

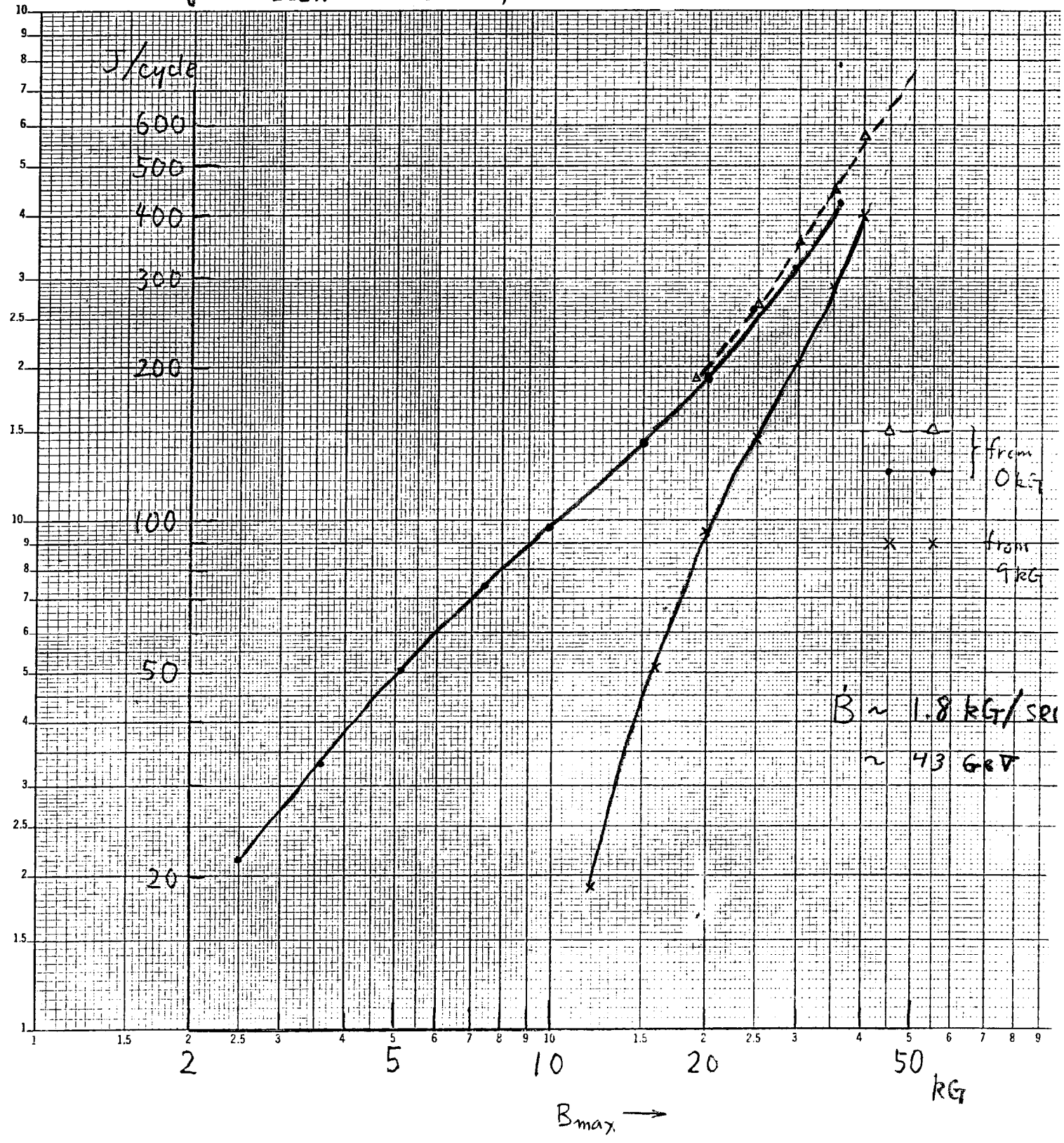


Aug 7, 1976

Fig 10 AC Loss of E22-1A



E-22-13 with Iron
Fig. 11 Max Field Dependence of AC Loss



E 22-13

3/4/77

$\tau = 24 \mu\text{sec}$

ducking ratio = c
= .013

X = 500A

Y = 5mV

int. 300ms

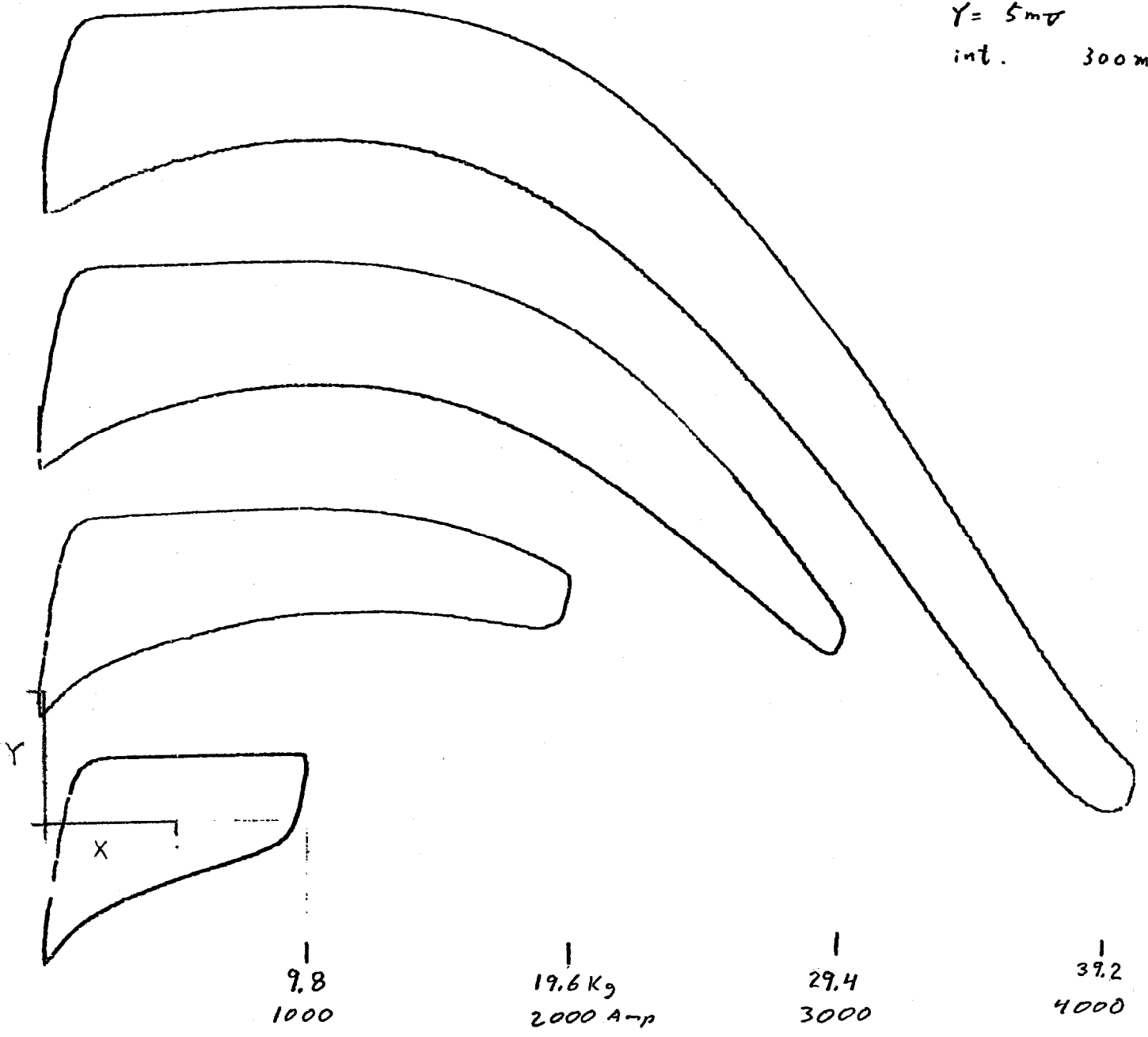


Fig. 12 Magnetization Curve of E22-13

Fig. 13 Axial Field Distribution of E-22-1A

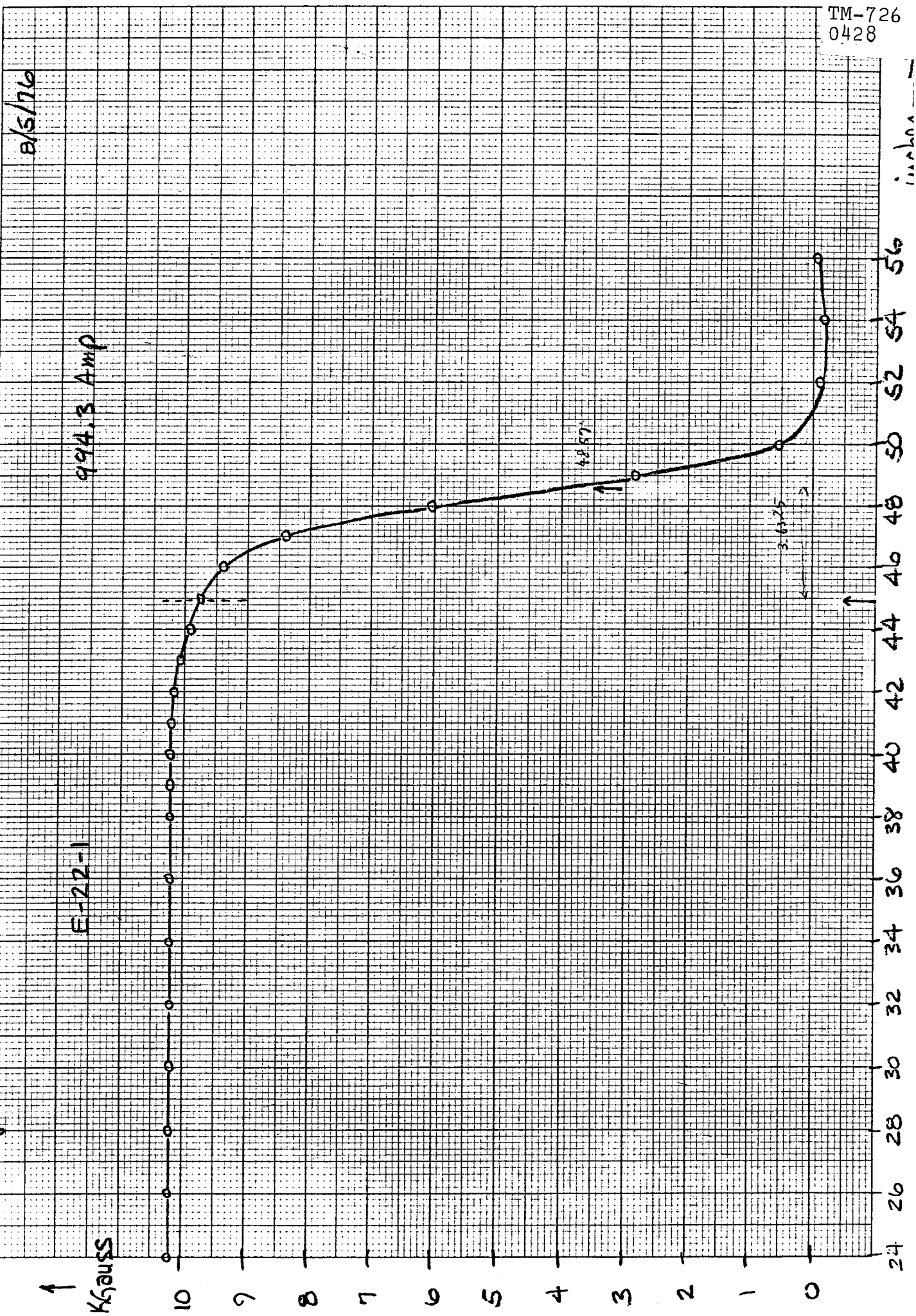
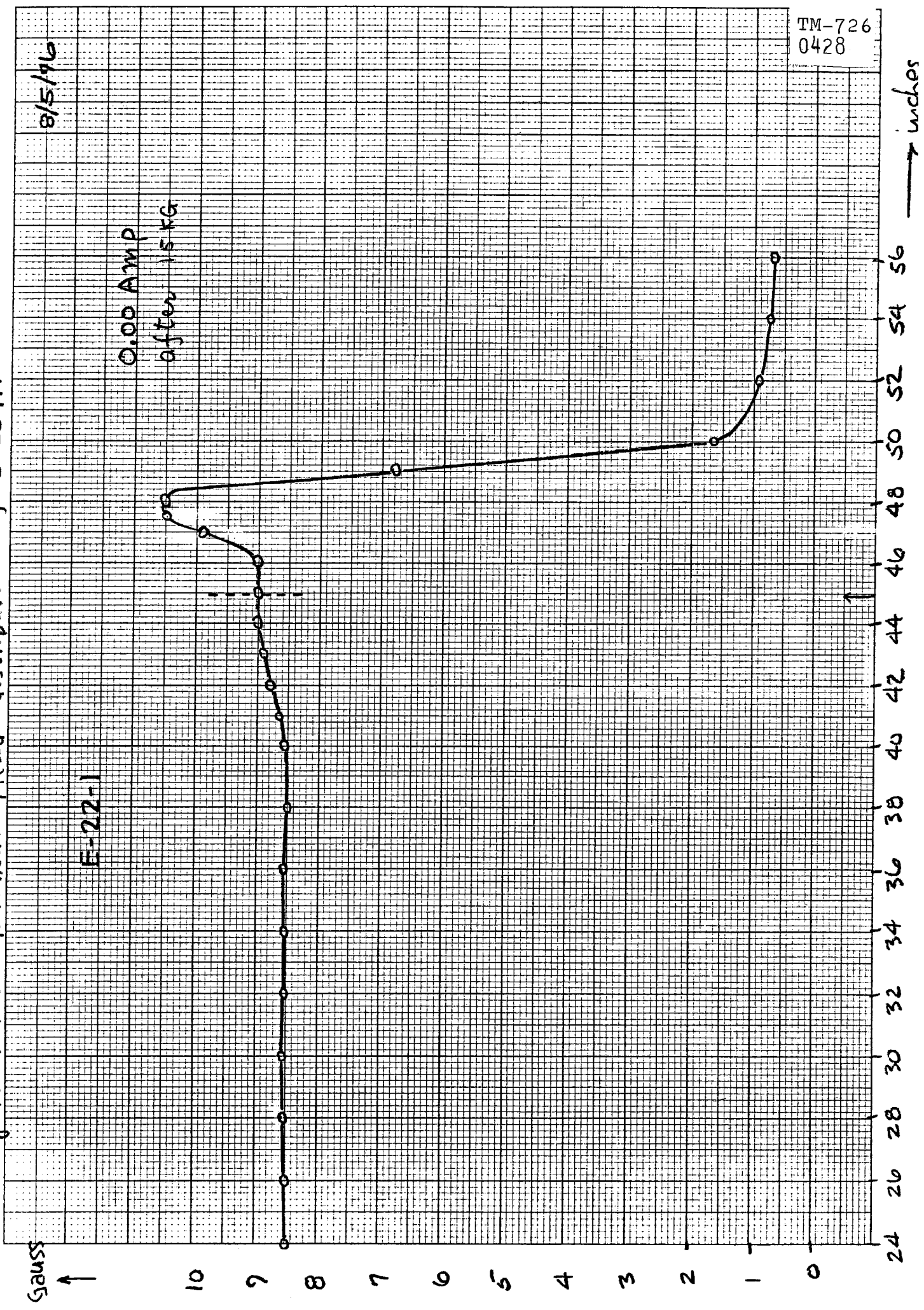


Fig. 14 Axial Remanent Field distribution of E 22-1A

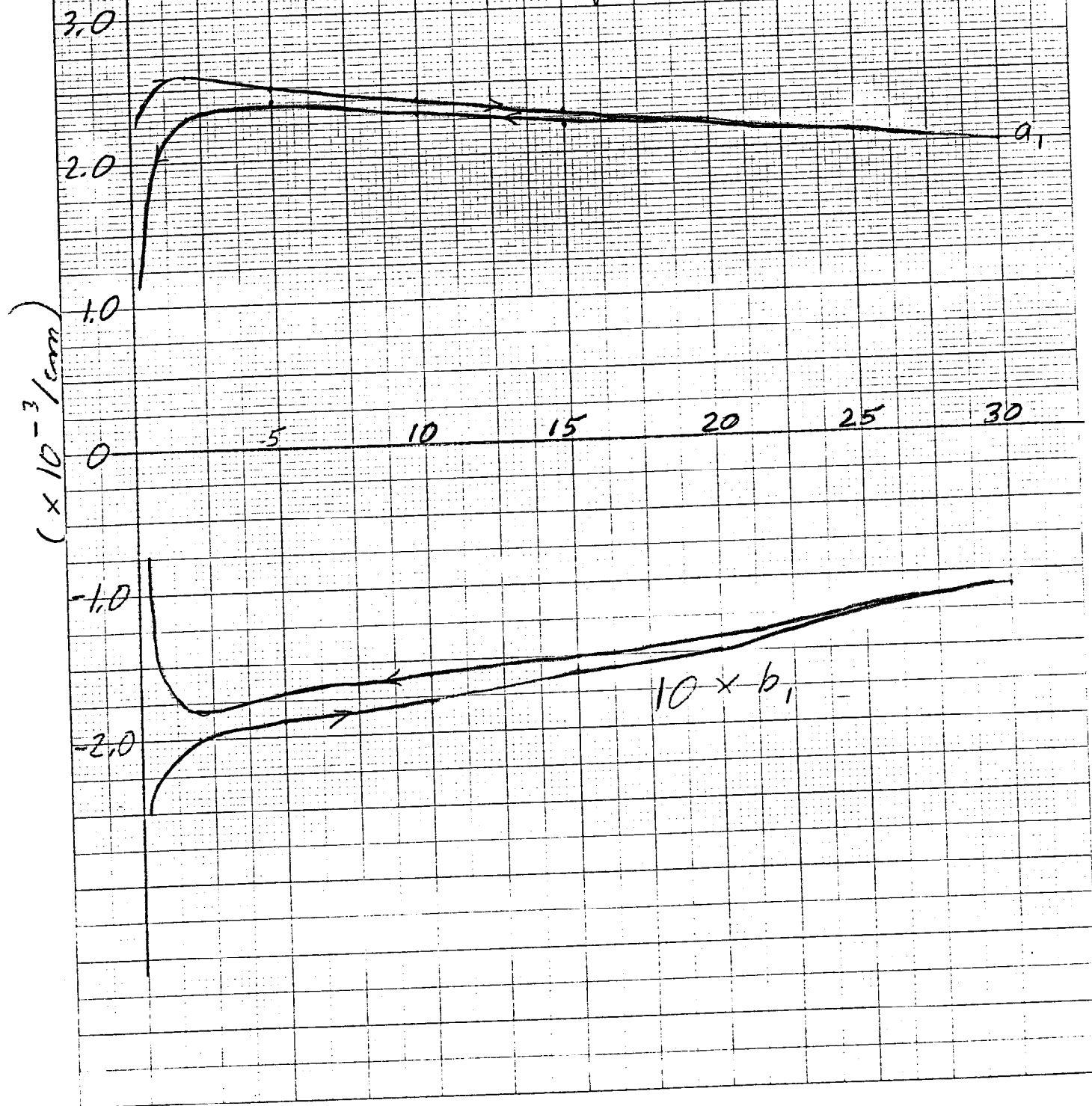


Aug 7 1976

Fig 15 E 22-1 Canned
DC 4-Pole Coefficients

$$B_y(y=0) = B_0(1 + b_1 x + b_2 x^2 + \dots)$$

$$B_x(y=0) = B_0(a_1 x + a_2 x^2 + \dots)$$



Aug 7

TM-726
0428

Fig 16

E 22-1 Canned

DC 6-Pole Coefficients

$(\times 10^{-3} / \text{cm}^2)$

5
4
3
2
1
0
-1
-2

Dipole Field (KG)

5 10 15 20 25 30

$10 \times a_2$

b_2

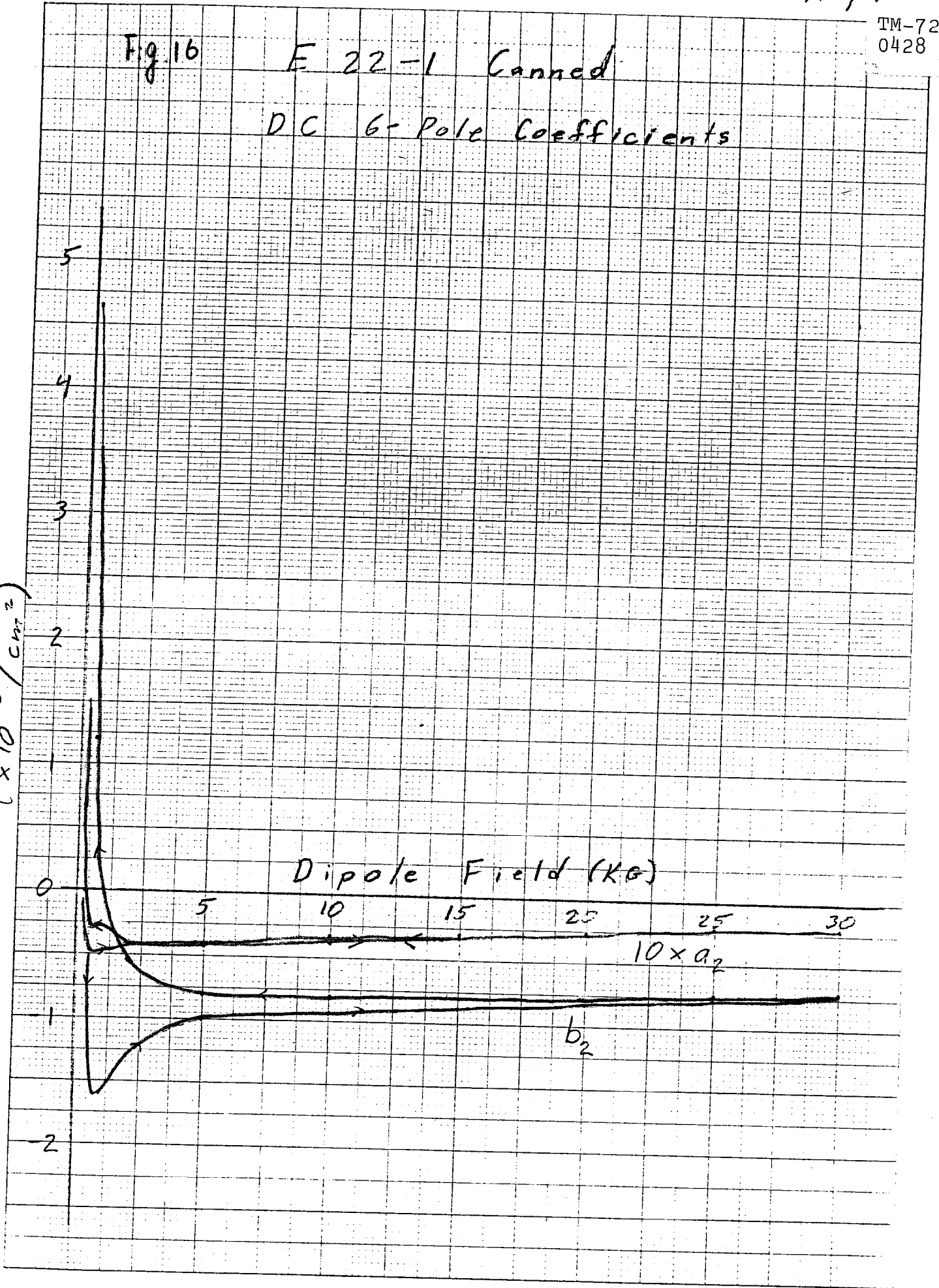
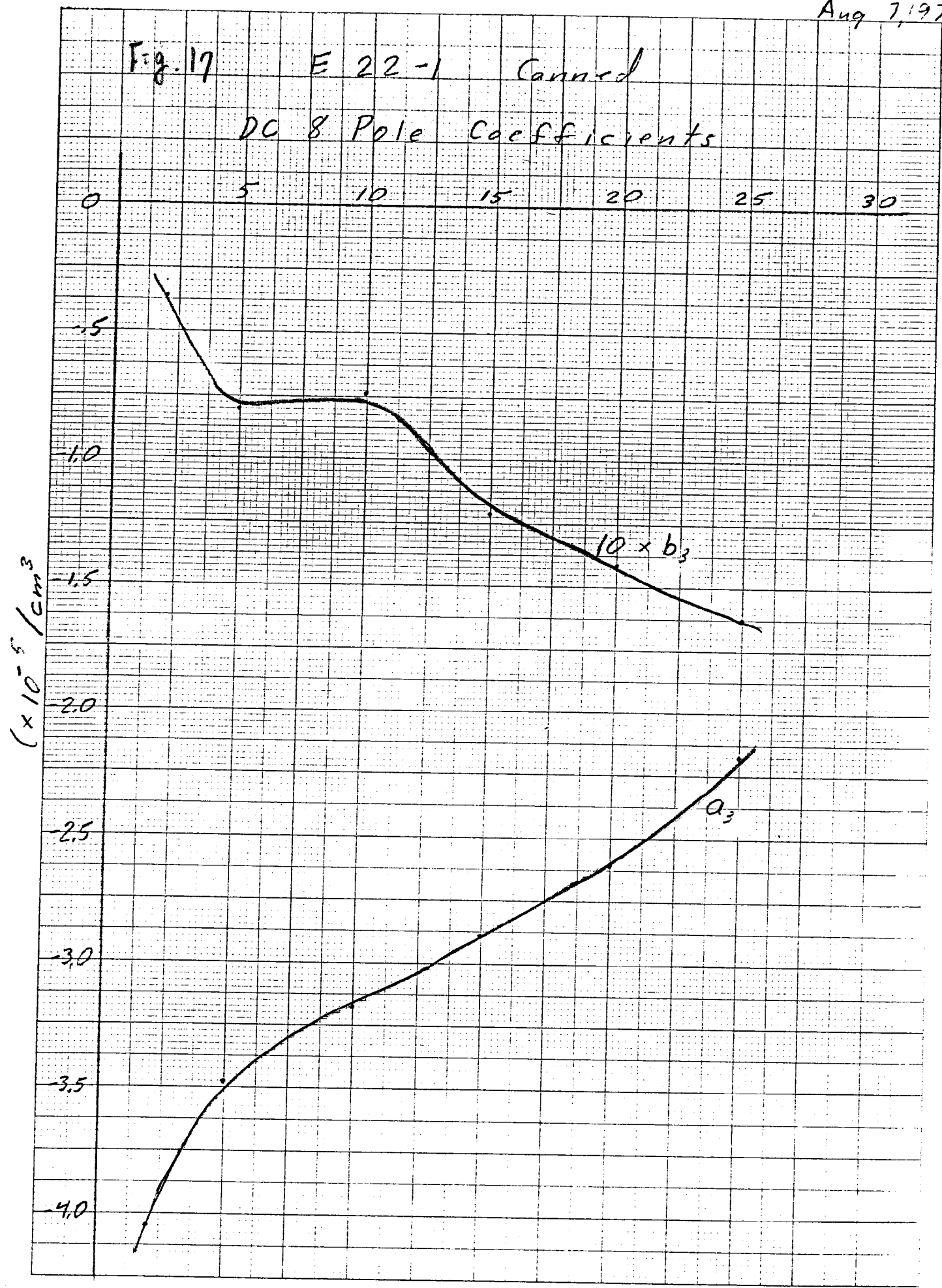


Fig. 17 E 22-1 Canned
DC 8 Pole Coefficients



Aug 7 1976

Fig. 18 E 22-1 Canned
DC 10 Pole Coefficients

($\times 10^{-5} / \text{cm}^4$)

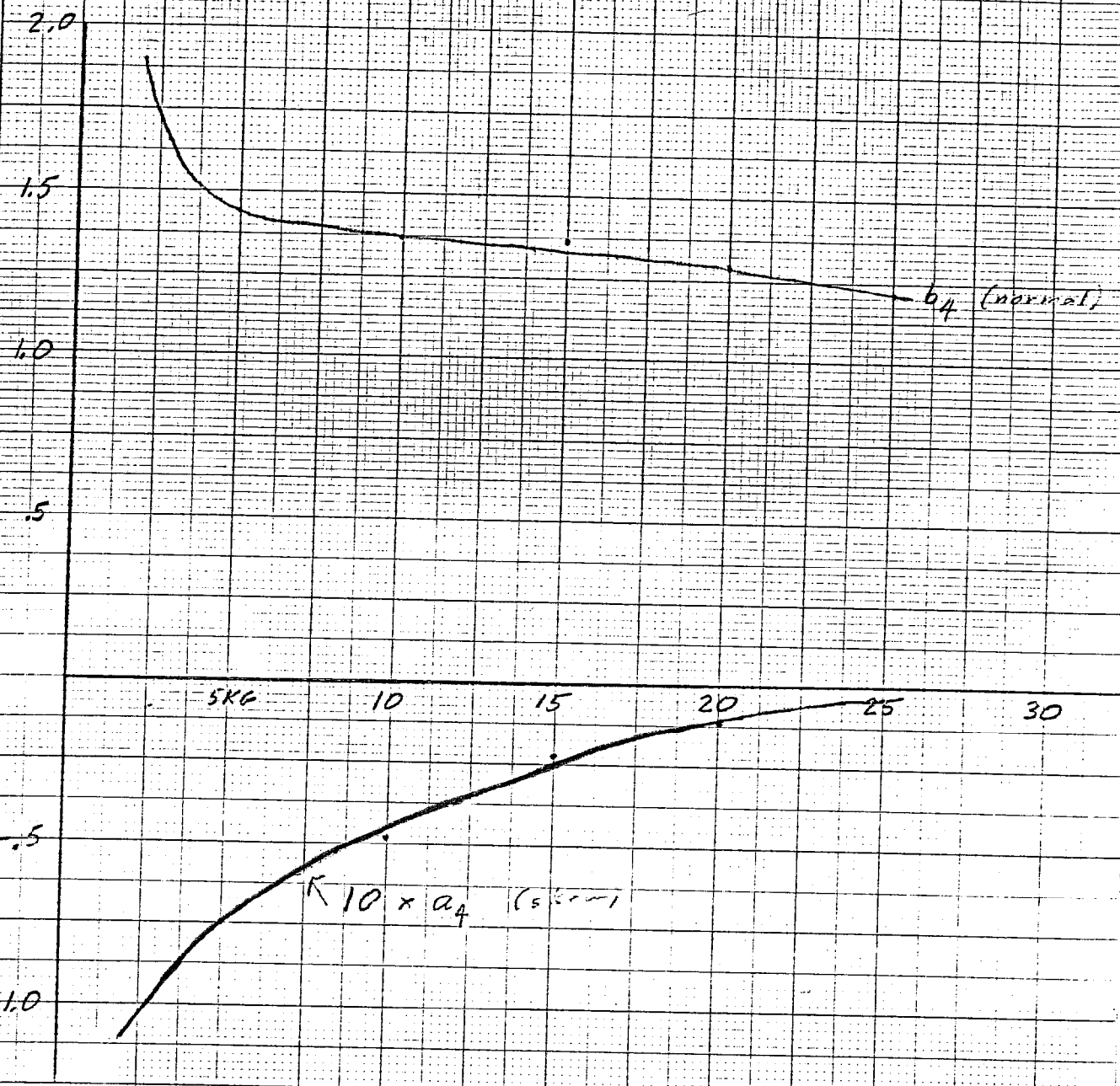


Fig 19 E - 22 - 13

4 pole

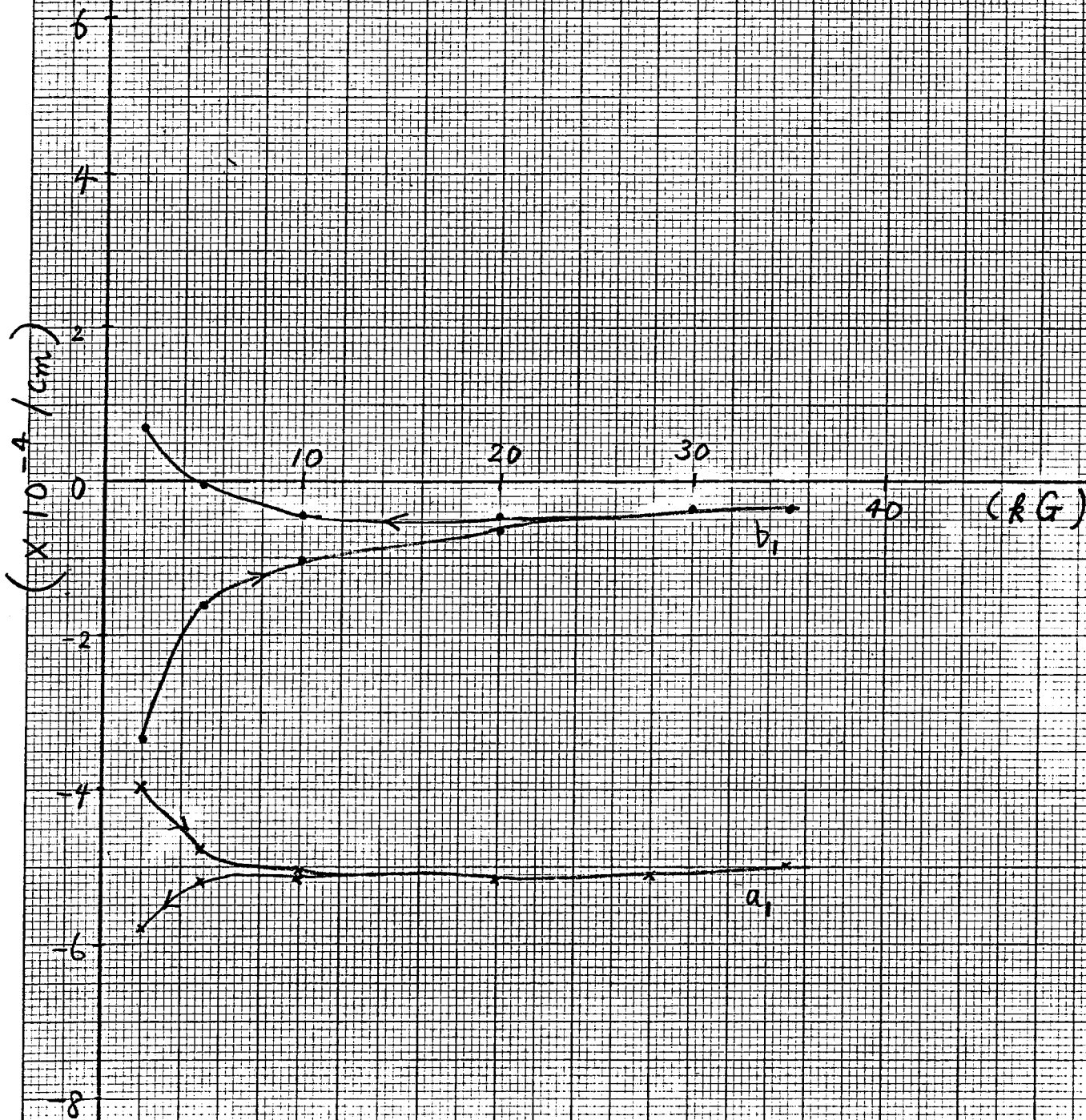


Fig 20 E-22-13

b pole

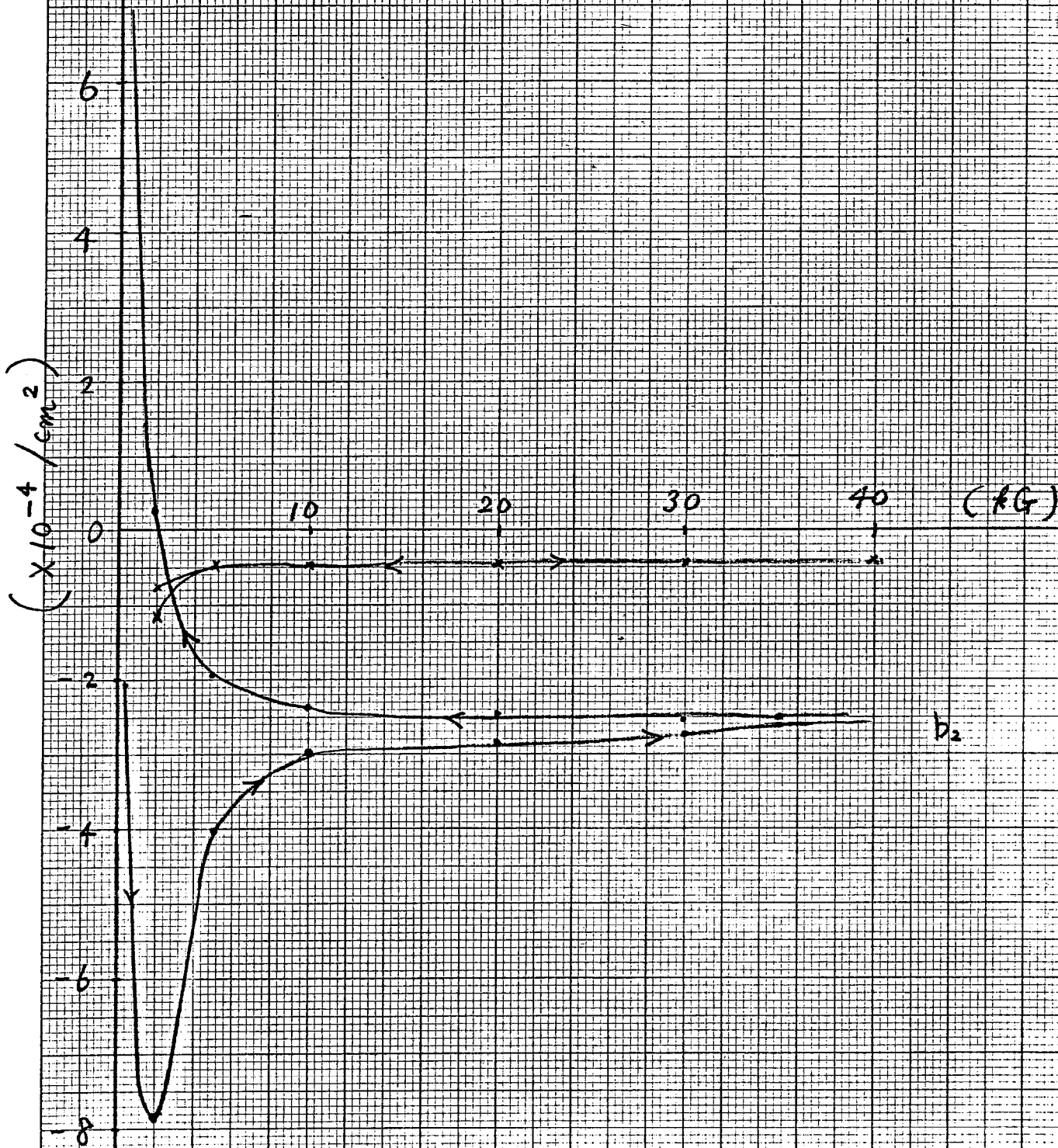
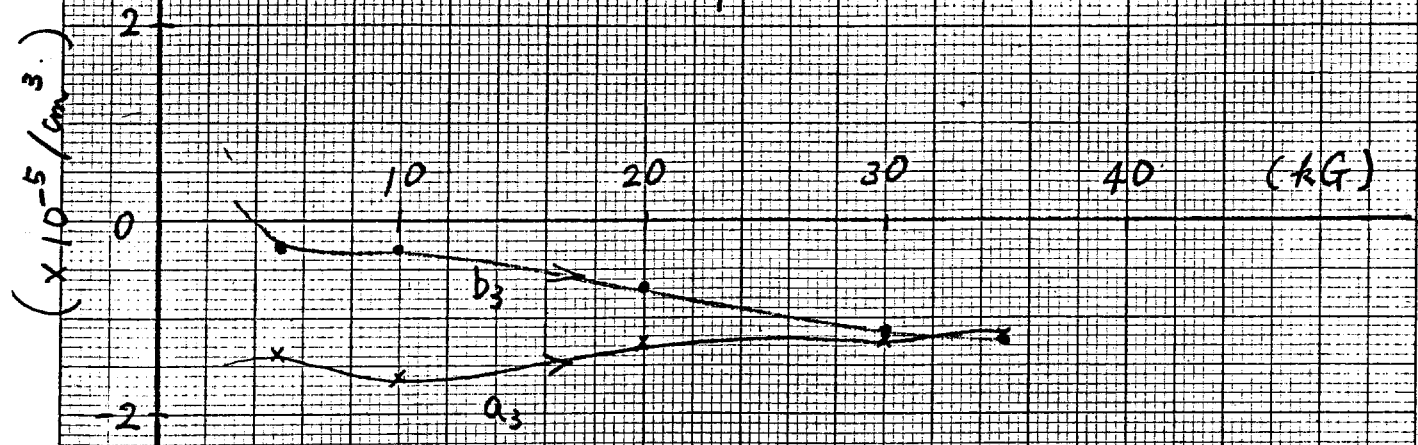


Fig 21 E-22-13
8 pole



10 pole

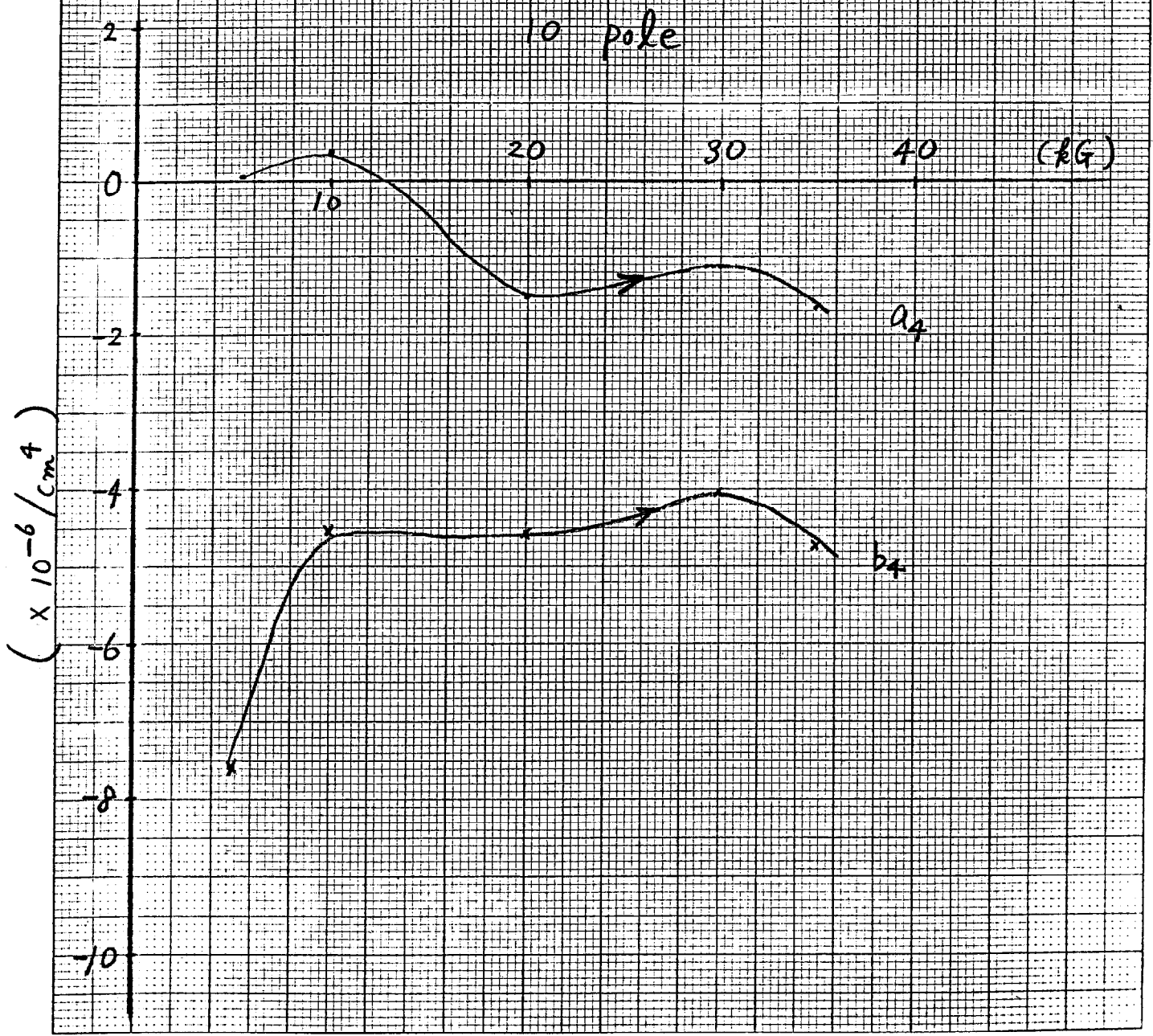


Fig 22

E 22-13

DC 6 Pole End Field

$\times 10^{-4} / \text{cm}^2$

2

0

-2

-4

-6

-8

-10

-12

-14

10

20

30

40

a_2

b_2

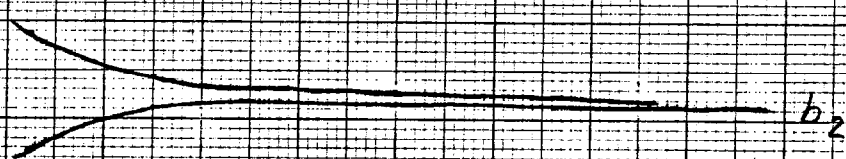
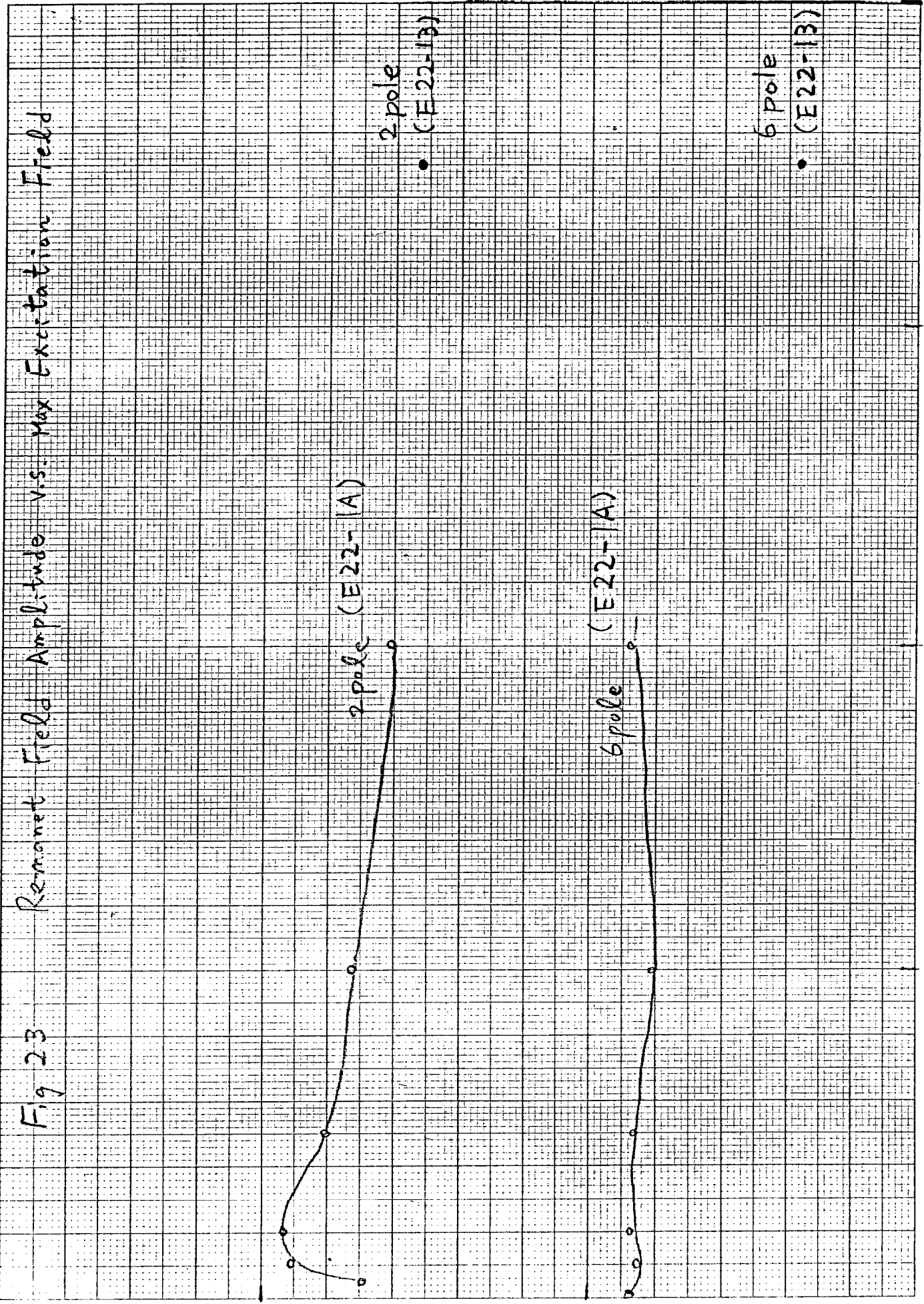


Fig 23 Remanent Field Amplitude v.s. Max Excitation Field



(gauss)

10

5

0

10

20

30

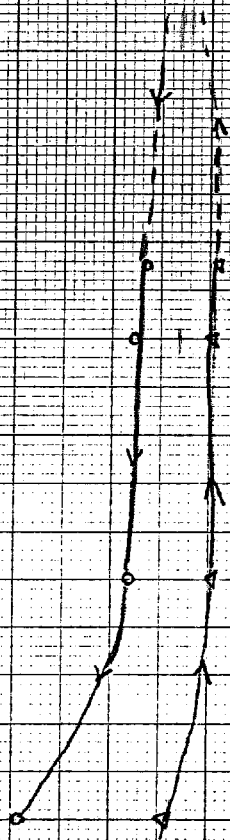
40

TM-726
0428

Transfer factor

E-22-13

Fig. 24



9.81

9.80

9.79

9.78

9.77

0

10

20

30

(KG)